A heat island model for large urban areas and its application to Milan (*)

S. BORGHI (1), G. CORBETTA (2) and L. DE BIASE (2)

(1) *Osservatorio Meteorologico, Milano-Duomo, Milano, Italy*
(2) *Dipartimento di Scienze dell'Ambiente e del Territorio, Università di Milano-Bicocca p.zza della Scienza 1, 20126 Milano, Italy*

(ricevuto il 25 Giugno 1999; revisionato il 12 Giugno 2000; approvato il 14 Luglio 2000)

Summary. — The study of the urban heat island has been carried out through two new enhanced versions of the UCLM (Urban Canopy Layer Model) model, Landsat/Thematic Mapper data sets and meteorological data collected over a square area 30 km of side including Milan and its hinterland. The urban climate can be described in different summer and winter radiative settings. The input data are divided into two classes: 1) parameters related to urban and rural local properties (albedo and emissivity, vegetation index NDVI, surface roughness length, land cover...); 2) meteorological data related to the general synoptic conditions. The bulk system of the model is made up of four independent equations expressed in terms of four unknowns, *i.e.*, the temperature values at ground level, canopy level and reference level (100 m) and relative humidity within the urban structure. The study area is divided by a regular square mesh of variable dimension (from 30 m to 1500 m); both the input and output data are average cell values. UCLM30 and UCLM60 calculate the temperature excess as well as the turbulent heat exchanges and the heat storage in the urban canopy as a function of the radiative and dynamic forcing. As can be observed in reality, the model shows that in summer the highest urban heating occurs in early morning and after sunset and that, in extreme conditions, the temperature can be up to 8 °C warmer in town than in the nearby rural lands.

PACS 92.60.Fm – Boundary layer structure and processes.

1. – Introduction

Urban settings of considerable dimensions usually bear dis-homogeneity, often relevant, in the distribution of micro-climatic features in the lower atmospheric layers; for example we all know that, in conditions of stability, in most urban areas the thermal

(*) The authors of this paper have agreed to not receive the proofs for correction.

phenomenon called *heat island* is observed, characterised by a distribution of increasing temperatures from the suburbs and surrounding rural areas to the centre of the metropolitan area [1-3]. The search of a method for the analysis of these thermic anomalies in different urban settings must take the different city climates and structures into account, together with the heterogeneity of urban surfaces. To this aim, it has been necessary to devise a technique both functional to a detailed analysis of the heat island and flexible enough to allow application to a wide range of different real settings.

For this reason, the analysis of the urban heat island in Milan has been carried out by means of the UCLM model (Urban Canopy Layer Model) modified by the authors of this paper in order to integrate satellite images [4], Fortran codes and meteorological data [5, 6]. The study of metropolitan climatology is profitably carried out only by means of a multidisciplinary approach that includes the selection of relevant input data, the parametrisation of physical processes [7] and the graphic elaboration of results [8]. The application of this model to the case of Milan gives interesting results in agreement with previous works [9, 10] concerning the heat island entity, extension and evolution.

2. – Input data acquisition

2·1. *The area.* – The region chosen for the study of the heat island is a square area 30 km of side including Milan and its hinterland (fig. 1). This area is divided by a regular square mesh; the dimension of the mesh can be varied from 30 m to 1500 m, depending on

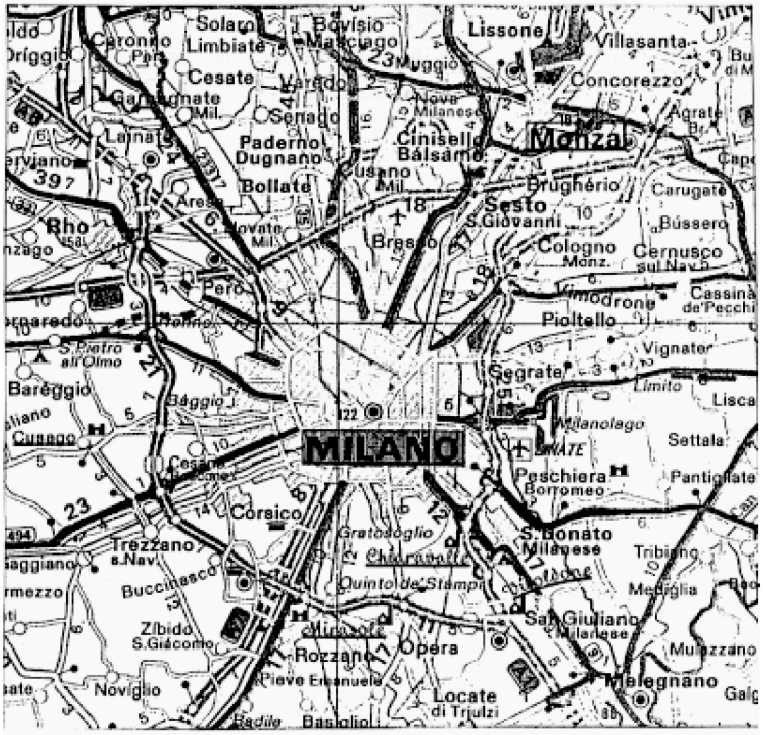

Fig. 1. – Area under study: Milan and its hinterland.

TABLE I. – *Cover classes based on spectral responses in Landsat TM channels.*

Cover land classes	Coverage percentage
Residential buildings	35%
Industrial areas	15%
Recent industrial areas (highly reflective)	5%
Vegetation	21%
Water	1%
Wet rural areas (rice fields, watered meadows, etc.)	5%
Rural areas (bare fields)	18%

the simulation purpose and modality. All input and output data are averaged on each cell of the mesh and considered as values taken at the central point of the cell. The relevant parameters for the cell are the thermic and hygrometric response.

2·2. *Input data.* – There are two classes of input data:

1) Parameters related to urban and rural local properties.

2) Meteorological data related to the general synoptic conditions.

Local properties for the area at study were reconstructed by means of remote sensing techniques on the basis of Landsat TM satellite images of May 1997 [11]. Such images were converted into numerical matrices; their entries were elaborated in such a way that, as a final result, it was possible:

– to detect 7 different land cover classes and their coverage percentage in the examined area (table I);

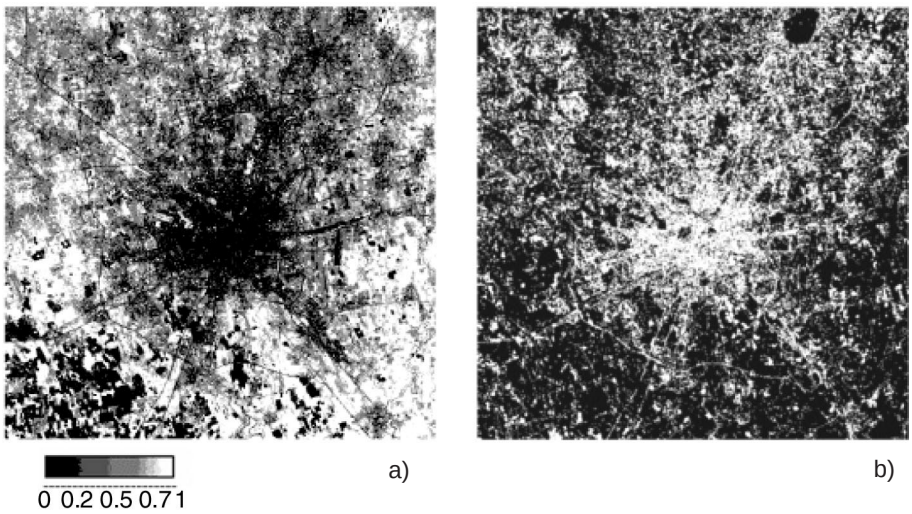

Fig. 2. – a) Albedo map and b) building density map (30 m spatial resolution) expressed as the ratio between the built area and the total area. The highly built-up areas, that is the white ones in b), have the lowest albedo values (darker in a)).

– to single out the building density σ_c (that is the ratio built area/total area), albedo (fig. 2) [12, 13] and vegetation index. There is a remarkable correlation between the highly built up areas of Milan and the lowest albedo values (the minimum is 0.08%);

– to assign specific emissivity and mean height values of the buildings. Each cover class is characterized by a specific kind of buildings with different height and material. The input meteorological data for the urban area result from the surface measurements recorded by the Milano-Duomo Meteorological Observatory; for the rural areas, the data were collected by radiosondes of Milano-Linate Meteorological Center.

3. – City modelling

The city structure, in the present study, is modelled as an ordered set of square blocks of different heights, grouped in bigger blocks spread uniformly in all the directions, according to the radial plant of Milan, and separated by «urban canyons» [6]. An urban canyon is a simple model of a main road. The buildings are aligned with continuity along its sides (fig. 3). In the model application the urban area is subdivided into square cells of given side. The buildings in each cell are assumed of equal height (the mean of the real heights, kindly provided by the local authorities). Several parameters can be chosen to describe the town in terms of its thermal behaviour. We briefly describe the main features of our city model, stressing, in particular, the new aspects with respect to the UCLM version by Castracane [6]. Our aim is to take into account the energetic balance relative to the surfaces of the buildings and of the ground together with the sensible and latent heat fluxes. Both radiation and heat fluxes are deeply affected by the geometric structure of the town. Let us discuss this dependence in some detail. Think of a single building, *i.e.* a parallelepiped with square basis of side t and height h. From now on we call surface A of the building the sum of the surfaces of all its sides, with the exception of its basis. During light hours, the bulding shades a portion A_h of the ground, depending on its dimensions and on the zenithal and azimuthal angles, θ and ϕ, respectively. We define the «shape factor» S_f as the ratio

$$S_f = A_h / A \,. \tag{1}$$

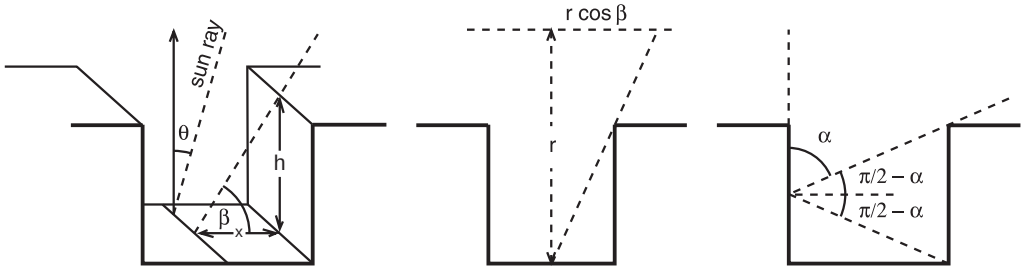

Fig. 3. – Urban canyon (width w and height h), on the left; canyon geometry, center, and view factor geometrical scheme, on the right.

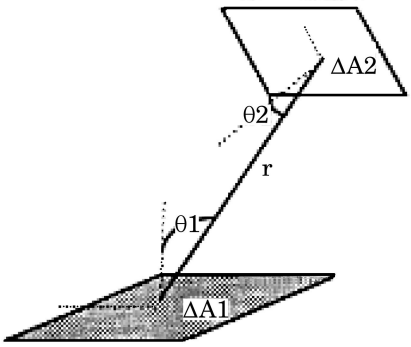

Fig. 4. – View factor geometry for two surfaces.

This factor has minimum value at 12 a.m. (when the only enlightened surface is the roof) and maximum values at sunrise and sunset.

We also define the "view factor" Ψ_{21} as the portion of the radiation emitted by a surface $\Delta A1$ which is intercepted by another surface $\Delta A2$ (fig. 4). It can be shown that if the positions of the surfaces $\Delta A1$ and $\Delta A2$ are as in fig. 4, its value is

$$(2) \qquad \Psi_{21} = \frac{\mathrm{rad}(\Delta A1)\cdot\Delta A2\cdot\cos(\theta_1)\cdot\cos(\theta_2)/r^2}{\pi\cdot\mathrm{rad}(\Delta A1)\cdot r^2} = \frac{\cos(\theta_1)\cdot\Delta A2\cdot\cos(\theta_2)}{\pi\cdot r^2},$$

depending only on the geometrical features and independent of the thermal properties. Finally we define the «sky» as an imaginary horizontal surface at the level of 100 m above the ground, where, on the basis of measured data, the interactions between the town and the atmosphere become much smaller than those analyzed in this paper. Thanks to this sort of lid of the city, the radiation emitted by a surface is totally intercepted by other surfaces: the ground, the sky, the neighbouring vertical surfaces.

3·1. *Radiative balance.* – The heat fluxes among the buildings (roof and walls), the soil and the sky have been estimated both in the long- and short-wave balance, denoted by «lw» and «sw», respectively. In our assumptions, all the buildings in the cell are of the same height, the view factors are reciprocally the same (that is $\Psi_{12} = \Psi_{21}$) and a urban canyon is defined by two walls, the ground and the sky.

In the short-wave balance, the radiation in a canyon is a function of the solar angle and of the geometric dimensions of the canyon itself; two are the possible situations:

1) Canyon bottom enlightened by a direct beam. The upward short-wave radiation includes the reflected part of the direct radiation intercepted by the building (roof and walls) and the diffuse light from the part of roof and walls not directly hit by light. The radiation coming from the soil is made up of the direct radiation from the enlightened area of the canyon bottom and the one diffused by the whole canyon bottom. In the short-wave balance, the fluxes [wall → wall] and [building → wall] are not explicitly expressed since their influence is included in the global balance, thanks to the shape and view factors (for example, the $[\text{walls} \rightarrow \text{sky}]_s$ flux is automatically related to the wall → wall interaction by the parameter Ψ_{sky}). Further studies to this aim are being carried out in order to improve the definition of fluxes inside the canopy, and not

only at the standard fixed levels $z = 0$ (ground), z_1 (building top) and z_2 (sky) as required by the present versions of UCLM. In this case, the short-wave radiation from the canyon bottom is

$$\text{Rsw} \uparrow = [\text{building} \rightarrow \text{sky}]_d + [\text{roof} \rightarrow \text{sky}]_s + [\text{wall} \rightarrow \text{sky}]_s + [\text{soil} \rightarrow \text{sky}]_d + [\text{soil} \rightarrow \text{sky}]_s , \tag{3}$$

where pedices d and s stand for direct and diffuse light. The term $[\text{building} \rightarrow \text{sky}]_d$ sums up the terms $[\text{wall} \rightarrow \text{sky}]_d$ and $[\text{roof} \rightarrow \text{sky}]_d$.

2) Canyon bottom in the shade; in this case

$$\text{Rsw} \uparrow = [\text{building} \rightarrow \text{sky}]_d + [\text{roof} \rightarrow \text{sky}]_s + [\text{wall} \rightarrow \text{sky}]_s + [\text{soil} \rightarrow \text{sky}]_s . \tag{4}$$

By summing all the relevant contributions, the net radiation balance is

$$\text{Rn} = \text{Rn}_c + \text{Rn}_g \tag{5}$$

where Rn_c and Rn_g are the net radiation at the buildings and ground level, respectively. The net radiation at the reference level (100 m above soil level) is

$$\text{Rn} = \text{Rsw} \downarrow - \text{Rsw} \uparrow + \text{Rlw} \downarrow - \text{Rlw} \uparrow . \tag{6}$$

Then the net radiation at the soil level is

$$\text{Rn}_g = \text{Rsw}_g \downarrow - \text{Rsw}_g \uparrow + \text{Rlw}_g \downarrow - \text{Rlw}_g \uparrow \tag{7}$$

The short-wave terms and their values are listed in table II; the long-wave balance is reported in table III.

The values of ε are different for different soil cover types, as reported in table IV [14, 15].

The emissivity of green areas is a function of the NDVI index [16, 17]:

$$\varepsilon = 1.0094 + 0.047 \cdot \ln(\text{NDVI}) . \tag{8}$$

The short-wave radiation $\text{Rsw} \downarrow$ is

$$\text{Rsw} \downarrow = \text{Rs}_0 \cdot [0.29 + 0.71 \cdot (1 - Cn)] , \tag{9}$$

where:

Rs_0 = solar radiation incident on a surface (in cloudless conditions),

Cn = index of cloud coverage (percentage).

TABLE II. – *Short-wave fluxes.*

$\text{Rsw} \downarrow = \text{Rsw}_d + \text{Rs}_s$	[sky → canyon]
$(1 - \sigma_c \cdot 5 \cdot S_f) \cdot \text{Rsw}_d$	$[\text{sky} \rightarrow \text{ground}]_d$
$(1 - \sigma_c) \cdot \Psi_{sky} \cdot \text{Rsw}_d$	$[\text{sky} \rightarrow \text{ground}]_s$
$(1 + 4 \cdot h/t) \cdot S_f \cdot \sigma_c \cdot \alpha_c \cdot \text{Rsw}_d$	$[\text{building} \rightarrow \text{sky}]_d$
$\sigma_c \cdot \alpha_c \cdot \text{Rsw}_s$	$[\text{roof} \rightarrow \text{sky}]_s$
$2 \cdot \sigma_c \cdot (h/t) \cdot \alpha_c \cdot \Psi_{wall} \cdot \text{Rs}_s$	$[\text{walls} \rightarrow \text{sky}]_s$
$\Psi_{sky}[\alpha_g \cdot (-4 \cdot h/t \cdot S_f \cdot \sigma_c) \cdot \text{Rsw}_d$	$[\text{ground} \rightarrow \text{sky}]_d$
$\alpha_g \cdot (1 - \sigma_c) \cdot \Psi_{sky} \cdot \text{Rsw}_s]$	$[\text{ground} \rightarrow \text{sky}]_s$

TABLE III. – *Long-wave fluxes.*

$\mathrm{Rlw}\downarrow = L\downarrow$	[sky → canyon]
$\Psi_{\mathrm{sky}}\cdot L\downarrow\cdot(1-\sigma_{\mathrm{c}})$	[sky→ground]
$2\Psi_{\mathrm{wall}}\cdot\sigma_{\mathrm{c}}\cdot\frac{h}{t}\cdot L_{\mathrm{c}}\downarrow$	[walls→ground]
$\sigma_{\mathrm{c}}\cdot[\varepsilon_{\mathrm{c}}\cdot\sigma\cdot T_{\mathrm{c}}^4+(1-\varepsilon)\cdot L\downarrow]$	[roof→sky]
$2\Psi_{\mathrm{wall}}\cdot\sigma_{\mathrm{c}}\cdot\frac{h}{t}\cdot[\varepsilon\cdot\sigma\cdot T_{\mathrm{c}}^4+(1-\varepsilon_{\mathrm{c}})\cdot L\downarrow]$	[walls→sky]
$(1-\sigma_{\mathrm{c}})\cdot\Psi_{\mathrm{sky}}\cdot[\varepsilon\cdot\sigma\cdot T_0^4+(1-\varepsilon)\cdot L\downarrow]$	[ground →sky]
$(1-\Psi_{\mathrm{sky}})\cdot(1-\sigma_{\mathrm{c}})\cdot L_{\mathrm{c}}\uparrow$	[ground →walls]

The long-wave radiation $L\downarrow$ from the atmosphere is given by

$$L\downarrow = \varepsilon_a\cdot\sigma\cdot T_2^4 \tag{10}$$

with ε_{a} = air emissivity [18], σ = Stefan-Boltzmann constant, T_2 = air temperature at level z_2.

The upward and downward fluxes $L_{\mathrm{c}}\uparrow$ and $L_{\mathrm{c}}\downarrow$ inside the canopy layer are described in a similar way.

3·2. *Energetic balance.* – The UCLM30 and UCLM60 mathematical structure consists of the solution of a system of four independent equations, concerning the different types of heat transport and storage. All these terms are computed at fixed levels (see fig. 5). The latent heat terms are negligible in this study since roofs and walls are assumed to be dry. The bulk system is:

1) $Q_{\mathrm{c}} = \mathrm{Rn}_{\mathrm{c}} - H_{\mathrm{c}} + Qa_{\mathrm{c}}$, Energetic balance at the building surface,
2) $Q_{\mathrm{g}} = \mathrm{Rn}_{\mathrm{g}} - H_{\mathrm{g}} - \lambda E_{\mathrm{g}} + Qa_{\mathrm{g}}$, Energetic balance at the soil surface,
3) $H_{\mathrm{a}} = H_{\mathrm{g}} + H_{\mathrm{c}}$, Sensible heat fluxes at the building top in fig. 5,
4) $E_{\mathrm{a}} = E_{\mathrm{g}}$, Latent heat fluxes at the building top in fig. 5.

TABLE IV. – *Emissivity values of different soil cover classes.*

Soil cover classes	Emissivity
Residential buildings	0.90
Industrial areas	0.85
Recent industrial areas (highly reflective)	0.8
Vegetation	in function of NDVI
Water	0.9
Wet rural areas (rice fields, watered meadows, etc.)	0.95
Rural areas (bare fields)	0.85

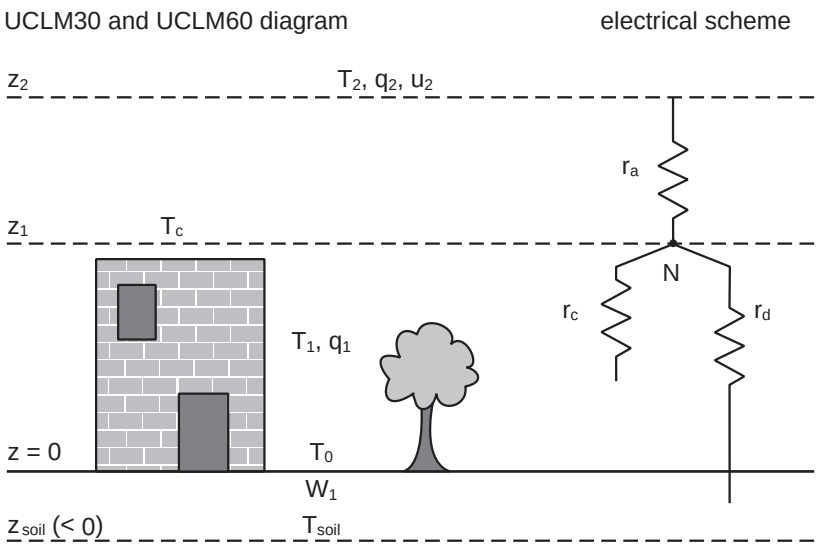

Fig. 5. – UCLM30 and UCLM60 structure and equivalent electrical scheme.

TABLE V. – *Thermal properties of materials used in building construction.*

Material (dry state)	c Specific heat (J kg^{-1} K^{-1} $\times 10^{-3}$)	C Heat capacity (J m^{-3} K^{-1} $\times 10^{-6}$)	k Thermal conductivity (W m^{-1} K^{-1})
Concrete	0.88	0.28	0.08
Stone	0.84	2.25	2.19
Brick	0.75	1.37	0.83
Wood	1.42	0.45	0.09
Steel	0.50	3.93	53.3
Glass	0.67	1.66	0.74

In the first equation of the bulk system, the different terms of heat transport and storage are considered. The conduction heat flow Q_c for buildings is defined as

$$Q_c = \mathrm{Rn}_c - H_c + Q\mathrm{a}_c. \tag{11}$$

The heat storage flux Q_i for buildings is supposed to be directly proportional to the direct radiation:

$$Q_i = D_c \cdot (\mathrm{Rn}_c + Q\mathrm{a}_c). \tag{12}$$

The coefficient D_c has different values for rural, suburban and urban areas and depends on the thermal properties of building materials reported in table V [19].

The sensible heat flux is expressed by the following equation:

$$H_c = \varrho \cdot c_p \cdot (T_c - T_1)/r_c, \tag{13}$$

where:
ϱ = wet air density (kg/m^3),

r_c = aerodynamic resistance at the interface building/air (s/m),
c_p = specific heat of wet air (J/kg · K).

The second equation deals with the energetic balance at the soil surface:

$$Q_g = \mathrm{Rn}_g - H_g - \lambda E_g + Q\mathrm{a}_g, \tag{14}$$

where:

Q_g = conduction heat flow in the terrain,
Rn_g = net radiation at the soil level (z_0),
H_g = sensible heat flux,
λE_g = latent heat flux at the interface air-soil (level z_0),
$Q\mathrm{a}_g$ = anthropogenic heat at the soil level.

The heat flux Q_g in the soil is strictly connected to the net radiation Rn_g:

$$Q_g = D_g \cdot (\mathrm{Rn}_g + Q\mathrm{a}_g)\,. \tag{15}$$

The coefficient D_g depends on the thermal properties of soil and land cover [20]. The sensible heat flux is

$$H_g = \varrho \cdot (T_0 - T_1)/r_d, \tag{16}$$

where r_{d0} is the aerodynamic resistance at the interface air/soil (level z_0).

The latent heat flux has been parametrised by the evaporation latent heat λ (J/Kg):

$$\lambda = (2501 - 2.\,3601 \cdot T_1) \cdot 10^3 \tag{17}$$

which multiplies the vapour flux:

$$E_g = \varrho \cdot (f_h \cdot q_{0s} - q_1)/(r_d + r_{soil})\,, \tag{18}$$

where:

f_h = air relative humidity at the soil level $z = 0$,
q_{0s} = specific humidity of saturated air (at T_0 temperature),
q_1 = specific humidity inside the canopy layer (between $z = 0$ and z_1 levels),
r_{soil} = aerodynamic resistance of the soil layer between $z = 0$ and z_{soil} levels.

The relationship between specific humidity and relative humidity and their values at the interface air/soil have been evaluated by applying the classical laws of meteorology and agronomy.

Finally, the anthropogenic heat $Q\mathrm{a}$ is [21, 22]:

$$Q\mathrm{a} = \begin{cases} H_1 + H_2 \cdot (291.5 - T_1) & T_1 < 291.5\,\mathrm{K}\,, \\ H_1 & T_1 \geqslant 291.5\,\mathrm{K}\,. \end{cases} \tag{19}$$

The empirical constant H_1 is influenced by the town size and by traffic and industrial activities. H_2 refers principally to domestic heating in winter and is relevant when $T_1 < 18.3\,^\circ\mathrm{C}$ [22].

The anthropogenic heat is split into two contributions, $Q\mathrm{a}_c$ and $Q\mathrm{a}_g$, relative to the canopy and soil levels, respectively:

$$Q\mathrm{a}_c = [3 \cdot \sigma_c/(1 + 2 \cdot \sigma_c)] \cdot Q\mathrm{a} \tag{20}$$

$$Q\mathrm{a}_g = [(1 - \sigma_c)/(1 + 2 \cdot \sigma_c)] \cdot Q\mathrm{a}\,. \tag{21}$$

TABLE VI. – *Electrical expression of heat fluxes.*

Flux	Coefficient	Intensity difference	Resistance
H_g	$\varrho \cdot C_p$	T_0-T_1	r_d
H_c	$\varrho \cdot C_p$	T_c-T_1	r_c
H_a	$\varrho \cdot C_p$	T_1-T_2	r_a
$\lambda \cdot E_g$	$\lambda \cdot \varrho$	$h \cdot q_{0s}$-q_1	$r_d + r_s$
$\lambda \cdot E_a$	$\lambda \cdot \varrho$	q_1-q_2	r_a

The data for the evaluation of anthropogenic heat were based on the actual fuel and electric annual consumption in the province of Milan.

In order to understand the third and fourth equations of the bulk system, a comparison is made between electrical and convective fluxes (table VI):

(22) flux *proportional to* (intensity difference/resistance).

Every level is assimilated to a node in an electrical network in which the sum of incoming fluxes equals the sum of outgoing ones. The resistances are placed at the interfaces soil/air (level z_0), building/air (in the canopy, at the building surface) and inside the soil (under the ground surface, level z_{soil}). At level z_1 and node 1, the equilibrium equation for sensible heat fluxes is

$$H_a = H_c + H_g, \tag{23}$$

where:

H_a = flux in the atmosphere layer $[z_1; z_2]$,
H_c = flux in the canopy layer $[z_1; z_0]$,
H_a = flux in the soil layer $[z_{soil}; z_0]$,
H_a is given by

$$H_a = \varrho \cdot C_p \cdot (T_1 - T_2)/r_a, \tag{24}$$

where r_a = aerodynamic resistance canopy/atmosphere (s/m).

The resistances are inversely proportional to the drag coefficients c_{dc} and c_{ds} and the wind intensity in the canopy layer [23]:

$$r_a = \frac{\sigma_c}{c_{dc}\, u_{ac}}, \tag{25}$$

$$r_c = \frac{1}{c_{dc}\, u_{ac}}, \tag{26}$$

$$r_d = \frac{1}{c_{ds}\, u_{ac}}, \tag{27}$$

where

r_c = aerodynamic resistance building/air inside the canopy layer,
r_d = aerodynamic resistance air/soil,
u_{ac} represents the wind intensity inside the canopy layer $[z_1; z_0]$ and takes into

account the mixed land cover of the urban canopy [24]:

$$u_{ac} = \sigma_c \cdot u_c + (1 - \sigma_c) \cdot u_2, \tag{28}$$

with u_2 = wind intensity at z_2 level (m/s), u_c = friction velocity (m/s).

The friction velocity u_c is a function of the drag coefficient c_{dc} and of the wind intensity u_2:

$$u_c = 0.83 \cdot (c_{dc})^{0.5} \cdot u_2. \tag{29}$$

The drag coefficients c_{dc} and c_{ds} are related to the built area (c is for canopy) and to the free soil (pedix g) [25]:

$$c_{dc} = \{K/\log[(z_2 - d)/z_{0c})]\}^2 \cdot \Phi_c(\mathrm{Ri}), \tag{30}$$

$$c_{dg} = [K/\log(z_2/z_{0g})]^2 \cdot \Phi_g(\mathrm{Ri}), \tag{31}$$

where:

$K = 0.41$ = von Karman constant,

z_{0c}, z_{0g} = roughness lengths for canopy and soil [26],

d = zero shift level (that is the imaginary base level of the friction force caused by the buildings on air).

A unique drag coefficient c_d is defined for the ground surface on the whole (built and non-built) areas by means of coefficient σ_c:

$$c_d = \sigma_c \cdot c_{dc} + (1 - \sigma_c) \cdot c_{dg}. \tag{32}$$

The stability function Φ_x (where the pedix x can be c or g) is represented as follows by introducing the parametrization suggested by [27, 28]:

$$\Phi_x = \begin{cases} 1/(1 + 4.7 \cdot \mathrm{Ri})]^2, & \mathrm{Ri} \geq 0, \\ [1 - 9.4 \cdot \mathrm{Ri}/(1 + 69.56 \cdot c_{dx} \cdot z_2/z_{0x} \cdot |\mathrm{Ri}|)] & \mathrm{Ri} < 0. \end{cases} \tag{33}$$

The Richardson number Ri depends on the temperatures at the building and soil surface, the coefficient σ_c and the wind intensity u_2.

Finally, the resistance r_s at the interface between the superficial soil layer and the deeper one (level z_{soil}) is defined by [29]:

$$r_s = \begin{cases} x_1 + x_2 \cdot W_1^{-2}, & q_{0s} \geq q_1, \\ 0, & q_{0s} < q_1, \end{cases} \tag{34}$$

where:

x_1, x_2 = parameters depending on the soil type,

W_1 = soil relative humidity,

q_{0s} = soil specific humidity,

q_1 = specific humidity at level z_1.

The parameters x_1 and x_2 for urban soils are taken from [29]. The values of soil relative humidity W_1 can be inferred from the graphs describing water extraction potential *vs.* water contents in soils with different textures. Some typical values of W_1 are 0.14 for urban areas, 0.29 for suburban ones and 0.33 for rural lands.

4. – Output elaboration

From the results of the UCLM system it is possible, for every cell of the mesh, to find:

1) the ground and building surface temperature;

2) the air temperature and humidity in the canopy layer, at an intermediate level between the soil and the top of the buildings (T_1) and at level z_1 (T_c).

The radiative and energetic fluxes are computed for every cell; the results (numerical matrices) are converted into black and white images thanks to a subroutine devised to this aim. The computing and graphical rendering of the intensity of the heat island (*i.e.* the difference between the urban temperature and the lowest rural temperature) is obtained by the application of a special Fortran code to the UCLM30 and UCLM60 temperature maps.

5. – A real example: the case of Milan

Milan is a large town in Northern Italy, hosting about 1.8 million residential inhabitants and the work activities of about 2.5 million people. Its climate is tipically continental, with cold and foggy winter and hot humid summer. Due to the shelter offered by the Alps on the northern side and by the Apennines on the southern one, together with the persistence of anticyclonic conditions, the wind is almost absent during most of the year (around 60% of the days [10, 30]). This leads to frequent occurrences of the heat island phenomenon. Some recent and real radiative situations of Milan (years 1997 and 1998) were chosen for the simulations; these situations are examples of calm atmospheric conditions with clear sky and moderate or light wind (0.2–3 m/s).

In the summer simulation (1998, August 28) two sample sites of $1.5 \times 1.5\ \mathrm{km}^2$ area have been selected; one near the Castello Sforzesco, in the centre of Milan, and a rural one near the town of Truccazzano. For each of them the application of UCLM gives the 24 hour trends of soil and air temperatures, heat transport and net radiation (fig. 6).

In the same day, the graphics and the photographic zoom from 300 to 30 m spatial resolution (fig. 7) show the presence of the heat island especially before dawn and after sunset. In particular, the zoom of the urban area points out the close relation between the temperature of the air in contact with the various surfaces and the cover materials (higher temperatures correspond to buildings and streets, lower ones to green areas).

The map in fig. 8 shows the temperature distribution on the whole $30 \times 30\ \mathrm{km}^2$ area for the simulation of 1998, August 22, h 21:00; the results of these simulations are compared to the temperature measurements by the local network for air quality monitoring. UCLM data agree with most of the monitoring stations records, especially for the central area of Milan, where the difference between the measured air temperatures and UCLM results is much less than 1 °C. (table VII). The code results were confirmed by real meteorological data from monitoring stations at the ground for other three simulations of summer and winter heat island events. Measured data generally agree with model results for at least 80% of the monitoring sites. If a restricted area is considered (for example, the centre of Milan), in most cases there is total correspondence between computed and measured temperatures (table VII). Another summer simulation starts from the meteorological conditions of 1988, August 7,

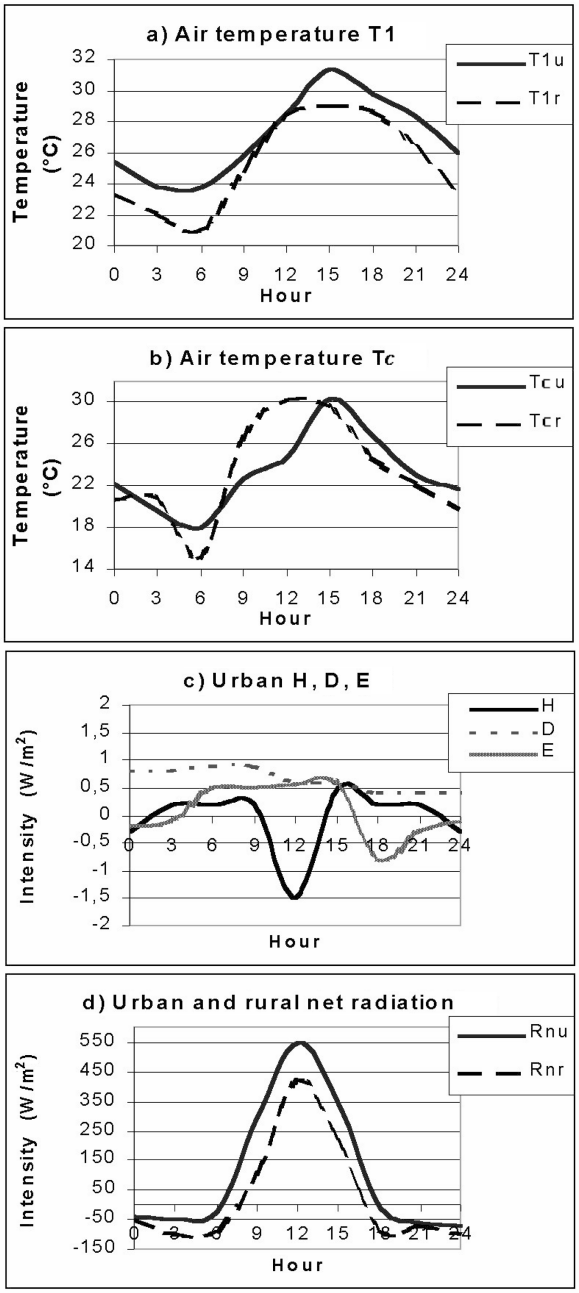

Fig. 6. – Simulation of 1998, August 28. Trends of air temperature T_1 (a) and T_c (b) (see fig. 5); trends of sensible (H), conduction (D) and latent (E) heat fluxes in the urban area (c); net radiation (d) in the urban and rural sample sites. The pedices «u» and «r» mean urban and rural, respectively.

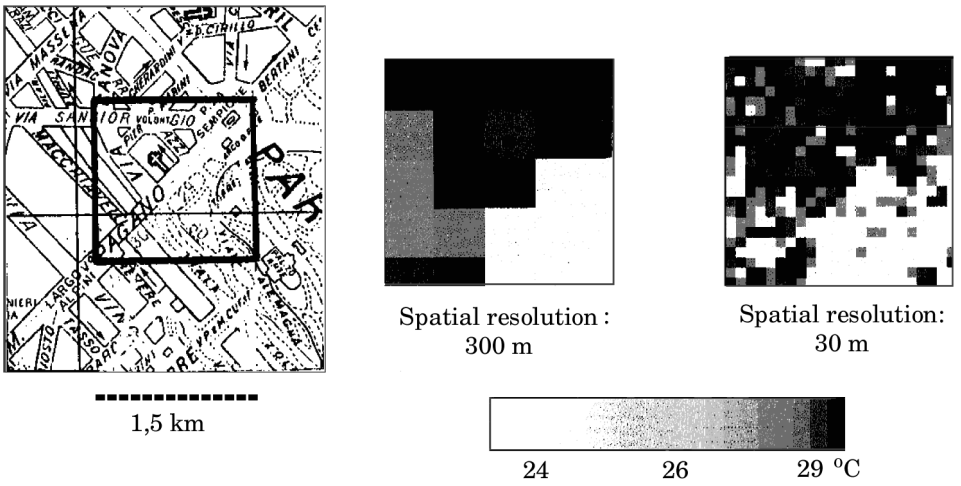

Fig. 7. – Zoom of the urban sample site near Castello Sforzesco up to 30 m spatial resolution (application of UCLM30) for the simulation of 1998, August 28, h 21:00; the influence of land cover on air temperature is straightforward.

a day with high temperature and weak wind; in this case, UCLM60 gives the daily evolution of the heat island on the whole area of interest (fig. 9). According to the results, there is a remarkable extension of the warmer plume towards the densely built

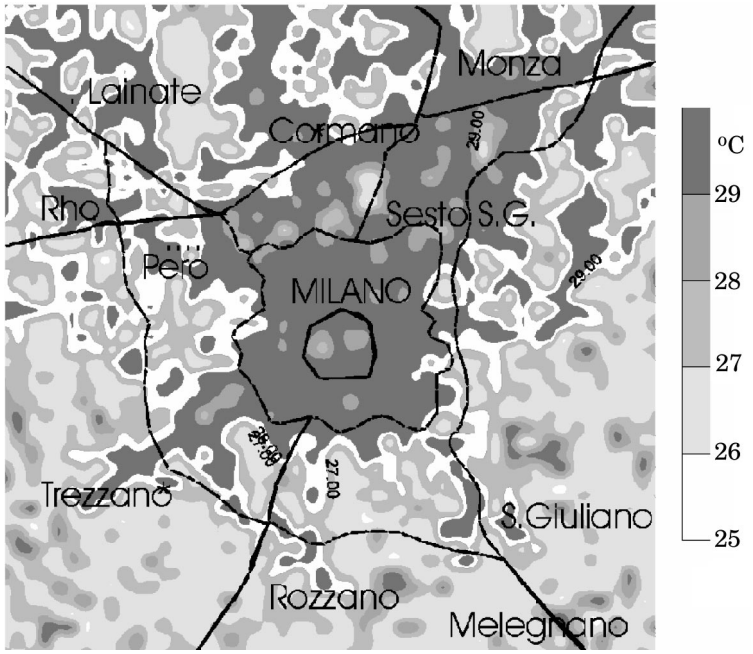

Fig. 8. – Map of the temperature at h 21:00 of 1998, August 28. The solid lines refer to the main motorways.

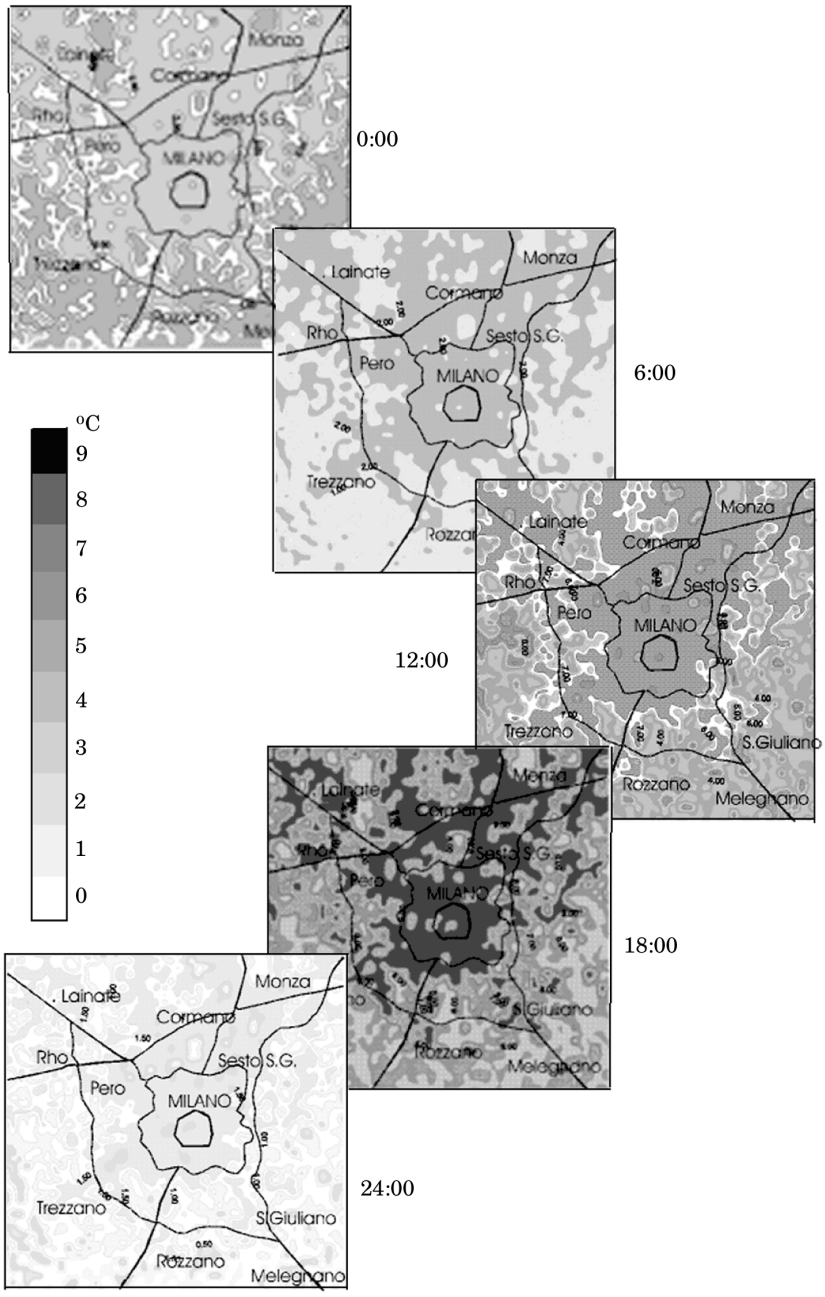

Fig. 9. – Evolution of the heat island intensity of 1998, August 7. The scale of grays indicates the temperature difference between the urban temperature and the lowest rural temperature.

TABLE VII. – *Comparison between measured air temperatures from the monitoring stations of PMIP network and UCLM output temperatures; simulation of 1998, August 22 h.21:00.*

PMIP station	Location	Measured T (°C)	UCLM T (°C)
Marche	centre of Milan	29.6	29.8
Juvara	centre of Milan	30.1	29.4
Zavattari	centre of Milan	30.2	29.9
Brera	centre of Milan	30.7	30.6
Monterho	NW hinterland	34.0	31.2
Agrate	NE hinterland	29.8	29.1
AEM quota	E hinterland	29.2	28.9
AEM suolo	E hinterland	29.6	29.3
Tavazzano	SE hinterland	32.1	34.3
Corsico	S hinterland	29.9	31.4

and industrialized North-East hinterland (Southern Brianza), with urban/rural temperature gap up to 8 °C.

The model sensitivity was tested by examining the results after an increase or decrease of the values of the key-parameters ($\pm 10\%$, $\pm 20\%$). This test displays the strong influence of wind intensity on UCLM output temperatures; in order to examine the relation, a foehn ([1]) event (1998, April 19) was selected to supply the meteorological input data for the simulation. This example clearly shows that moderate wind intensity cuts down urban/rural temperature differences from 4-5 °C to 1-2 °C and eliminates the heat island effect. UCLM30 and UCLM60 reliability is confirmed by previous studies about the heat island in Milan [2]; indeed, in 1993, the temperature difference between the stations of Milano-Duomo (in the centre of Milan) and Milano-Linate (in the suburbs) was already remarkable (7-8 °C) in the presence of persistent meteorological stability [9]. Other parametrs which strongly affect the model output temperatures are those connected with building density (σ_c) and thermal properties of materials (D_c, D_g). A slight variation ($\pm 10\%$) in σ_c, D_c or D_g value brings about considerable changes ($>10\%$) in the output air temperatures T_0, T_1 and T_c. This remark shows the effect of urbanization on the micrometeorology of densely built areas.

6. – Conclusions

According to the simulation results and to their comparison with meteorological data from monitoring stations in Milan, the models UCLM30 and UCLM60 can be considered useful tools for micro-meteorological studies in highly complex and heterogenous urban areas. More generally, an integration of remote sensing techniques, meteorological measurements and modelling turns out to be a valuable method for heat island analysis in different urban settings. The application of a simpler version of UCLM to the areas of Rome and Ljubljana has already given good results;

([1]) Typical dry wind which develops on the lee of the Alps where humidity is released by precipitation on the windward side of the mountain chain.

the method could therefore be a first step towards finding a standard approach to the study and modelling of the heat island. Other possible applications could be in the energetic field, principally to evaluate the heating and air-conditioning consumption in relation to the differential heating due to the *heat island* effect.

Appendix A

List of symbols

Latin symbols

A	sum of the surfaces of all the sides of a building, with the exception of its basis
A_h	portion of the ground shaded by the building
c_d	drag coefficient
c_p	specific heat of wet air
Cn	index of cloud coverage (percentage)
d	zero plane displacement
D_c	coefficient depending on the thermal properties of building materials
D_g	coefficient depending on the thermal properties of soil
E	latent heat flux
f_h	relative humidity of soil first layer
H	sensible heat flux
H_1 and H_2	empirical constants related to anthropogenic heat
h	height of buildings
K	von Karman constant
Qa	anthropogenic heat
Q	conduction heat flux (c-buildings, g-ground, a-air level)
q_{0s}	specific soil humidity
q_1	specific air humidity in the canopy layer
q_2	specific air humidity at level z_2
r_a	aerodynamic air resistance
r_c	aerodynamic resistance building-air
r_d	resistance soil-atmosphere
Ri	Richardson number
Rlw $\downarrow$	long-wave radiation from the atmosphere
Rlw $\uparrow$	long-wave radiation towards the atmosphere
$\mathrm{Rlw_g}\downarrow$	long-wave radiation from the atmosphere at the soil level
$\mathrm{Rlw_g}\uparrow$	long-wave radiation towards the atmosphere at the soil level
Rn	net radiation
$\mathrm{Rn_g}$	net radiation at the soil level
Rsw $\downarrow$	short-wave radiation from the atmosphere
Rsw $\uparrow$	short-wave radiation towards the atmosphere
$\mathrm{Rsw_g}\downarrow$	short-wave radiation from the atmosphere at the soil level
$\mathrm{Rsw_g}\uparrow$	short-wave radiation towards the atmosphere at the soil level
S_f	shape factor
t	side of the square basis of buildings (represented as rectangular blocks of variable heights)
T_0	air temperature at level $z = 0$
T_1	air temperature in the canopy layer
T_2	air temperature at level z_2

T_c	air temperature at level z_1
T_{soil}	soil temperature at level z_{soil}
u_{ac}	air/canopy wind velocity
u_c	friction velocity
u_2	wind velocity at level z_2
w	canyon width
$z=0, z_{soil}, z_1 z_2$	reference levels
z_0	roughness length
W_1	relative soil humidity
x_1, x_2	parameters for soil resistance

Greek symbols

α	angle of ϕ_{wall} factor
α_c or α_g	albedo for different land covers
β	angle depending on the canyon width w and the height of buildings h
ε	emissivity (of different land cover)
θ	zenithal angle
λ	soil heat conductivity
ϱ	wet air density
Ψ	view factor
σ	Stefan-Boltzmann constant
σ_c	ratio between the built area and the total area

List of the most used subscripts

a	related to the air of the layer between z_1 and z_2 levels
ac	related to the air within the urban canopy
c	related to the urban canopy
g (or s)	related to the soil, terrain
soil	related to the superficial layer of soil
0	related to $z = 0$ level
1	related to z_1 level
2	related to z_2 level

* * *

This work was partly supported by the contribution of the Environment Councelor of the Province of Milan.

The authors wish to thank the staff of the Meteorological Observatory Milano-Duomo and the Department of Environmental Sciences of Milano-Bicocca University for the help and support during this work. Special thanks to the G-Met of the Physics Department of the University «La Sapienza» in Rome for their valuable collaboration. Finally, sincere thanks to G. GUERRA for his patient and crucial help.

REFERENCES

[1] ATWATER M. A., *The radiation budget for polluted layers of the urban environment*, *J. Appl. Met.*, **14** (1971) 205-214.

[2] ATWATER M. A., *Thermal effects of urbanization and industrialization in the boundary layer: a numerical study*, *Boundary Layer Meteorol.*, **3** (1972) 229-245.

[3] KIM H. H., *Urban heat island*, *Int. J. Remote Sensing*, **13** (1992) 2319-2336.

[4] BALLINE R. C. and BRAZEL S. W., *High resolution surface temperature patterns in a complex urban terrain*, *Photogramm. Engin. Remote Sensing*, **9** (1988) 1289-1293.
[5] CASSARDO C., *Il Land Surface Process Model: un modello fisico per lo studio del bilancio energetico, termico ed idrologico tra il suolo e la bassa atmosfera*, Ph. D. Thesis, Università di Genova, Modena e Torino (1992).
[6] CASTRACANE P., *Un modello di bilanci radiativi per lo studio della canopia urbana*, Tesi di Laurea, Università di Roma "La Sapienza" (1996).
[7] DEARDOFF J. W., *Efficient prediction of ground surface temperature and moisture, with inclusion of a layer of vegetation*, *J. Geophys. Res. C*, **4** (1978) 1889-1903.
[8] ABBATE G., *Heat island study in the area of Roma by integrated use of ERS-SAR and Landsat TM data*, *Earthnet on line* (1998).
[9] BELLONI L., *L'isola di calore sull'area di Milano in relazione al regime circolatorio nella bassa troposfera*, Tesi di Laurea, Università di Milano (1993).
[10] BORGHI S. and GIULIACCI M., *Circulation features driven by diurnal heating in the lower atmospheric layers of the Po valley*, *Nuovo Cimento C*, **3** (1980) 1-16.
[11] PARLOW E. and SCHERER D., *Satellite based climate analysis of Basel/Switzerland*, in *Proceedings of the 3rd Symposium on "Space at the service of our environment", Florence, Italy* (1997).
[12] BREST C. and GOWARD S. N., *Deriving surface albedo measurements from narrow based satellite data*, *Int. J. Remote Sensing*, 8 (1987) 351-367.
[13] DUGUAY C. R., *Estimating surface reflectance and albedo from Landsat 5 Thematic Mapper over rugged terrain*, *Photogramm. Engin. Remote Sensing*, **8** (1992) 551-558.
[14] NICHOL J. E., *A GIS-based approach to microclimate monitoring in Singapore's high-rise housing estates*, *Photogramm. Engin. Remote Sensing*, **10** (1994) 1225-1232.
[15] RUBIO E., CASELLES V. and BADENAS C., *Emissivity measurements of several soils and vegetation types in the 8-14* μm *wave band: analysis of two field methods*, *Remote Sensing Environ.*, **59** (1997) 490-521.
[16] VALOR E. and CASELLES V., *Mapping land surface emissivity from NDVI: application to European, African and South American areas*, *Remote Sensing Environ.*, **57** (1994) 167-184.
[17] VAN DE GRIEND A. A. and OWE M., *On the relationship between thermal emissivity and the normalized difference vegetation index for natural surfaces*, *Int. J. Remote Sensing*, **6** (1993) 1119-1131.
[18] STALEY D. O. and JURICA G. M., *Effective atmosphere emissivity under clear skies*, *J. Appl. Meteorol.*, **11** (1972) 349-355.
[19] OKE T. R., *Boundary layer climates*, Second edition (Routledge) 1987.
[20] OKE T. R., *The energetic basis of urban heat island*, *Quart. J. R. Meteorol. Soc.*, **108** (1980) 1-24.
[21] ATWATER M. A., *Thermal changes induced by urbanization and pollutants*, *J. Appl. Meteorol.*, **14** (1975) 1061-1071.
[22] BENNETT M. and SAAB A. E., *Modelling of the urban heat island and of its interaction with pollutant dispersal*, *Atmosph. Environ.*, **16** (1982) 1797-1822.
[23] JI J. J. and HU. Y., *A simple land surface model for use in climate study*, *Acta Meteorol. Sinica*, **3** (1989) 344-353.
[24] LEGG B. J. and LONG I. F., *Turbulent diffusion within a wheat canopy II*, *Quart. J. R. Meteorol. Soc.*, **101** (1975) 611-628.
[25] VAN ULDEN A. P. and HOLTSLAG A. A. M., *Estimation of atmospheric boundary layer parametrs for diffusion applications*, *J. Climate Appl. Meteorol.*, **2** (1985) 1196-1207.
[26] VAN VEDEN A. P. and HOETSLAG A. A. M., *Estimation of atmospheric boundary layer parameters for diffusion applications*, *J. Climate Appl. Meteorol.*, **24** (1985) 1196-1207.
[27] LOUIS J. F., TIEDKE M. and GELEYINR J. F., *A short history of the PBL parametrization at EMWF*, *Workshop on PBL parametrization, ECMWF* (1981) 59-79.

[28] ANDRÈ J. C., *Multi-level boundary layer scheme, physical parametrization for numerical models of the atmosphere*, *ECMWF Seminar* (1985) 33-34.
[29] LIN J. D. and SUN S. F., *A method for coupling parametrization of the planetary boundary layer with a hydrologic model*, *Climate Appl. Meteorol.*, **25** (1986) 1971-1976.
[30] BORGHI S. *et al.*, *Analysis of Lombardia's rainfall and of its relationship with the atmospheric circulation at 850 hPa*, in *Proceedings of the International Conference on Application of time series analysis in Astronomy and Meteorology, University of Padua, Italy* (1993), pp. 343-346.